

Phase-field Study of Plateau-Rayleigh Instability in Multilayer Nanocrystalline Thin Film

Tamoghna Chakrabarti^{a,*}, Nisha Verma^{b,d}, Sukriti Manna^{c,d,*}

^a*Department of Metallurgical and Materials Engineering, Colorado School of Mines, Golden, CO 80401, USA*

^b*Department of Materials Science and Engineering, University of Illinois at Urbana-Champaign, IL 61801, USA*

^c*Department of Materials Engineering, Indian Institute of Science, Bangalore 560012, India*

^d*Department of Mechanical Engineering, Colorado School of Mines, Golden, CO 80401, USA*

Abstract

Thermal stability of nanocrystalline multilayer thin film is of paramount importance as the applications often involve high temperature. We have studied the stability of multilayer thin film using phase-field simulations. Effect of layer thickness, bilayer spacing, the presence of grain boundary and grain boundary mobilities of individual phases on the layer stability have been explored in this work. Layer instability in the polycrystalline film is shown to arise from the grain boundary grooving followed by Plateau-Rayleigh instability. Increase in layer thickness, lower bilayer thickness as well as lower grain boundary mobility improve layer stability. Phase-field simulations show similar microstructural evolution as has been observed in our Zirconium (Zr)/Zirconium Nitride (ZrN) system experimentally. Detail analysis performed in this work to understand the mechanisms of layer instability leads us to predict measures which will improve the thermal stability of multilayer nanocrystalline thin film.

Keywords:

multilayer, coating, thermal stability, nanocrystalline, thin film, phase-field, Plateau-Rayleigh instability

1. Introduction

Multilayer thin films are assemblage of alternate stacking of two phases with desirable properties. Multilayer thin films are successfully applied as surface protection for tribological applications, diffusion barriers in microelectronics, hard wear resistant coatings on cutting tools due to their high hardness, fracture toughness, chemical inertness and thermal stability. [1, 2, 3]. Essentially, the designing of an appropriate microstructure is the key for desired thin film properties. Multilayer shows better performance compared to single layer film. The design with metal/nitride multilayer coating show improved fracture resistance without much compromise of hardness [4, 5, 6, 7], implying the desirable properties are an outcome of reduction in grain size and increased number of interfaces.

The thermal stability is defined as deterioration of properties as a function of temperature, involving changes in microstructure, grain growth, composition, phase transformation and oxidation. Most of the multilayer thin film coatings are used for tribological application owing to their superior mechanical properties. During such tribological applications, temperature in the coated work piece can rise to very high temperature of around 1000°C. High temperature generated during the operation may lead to grain coarsening and disintegration of the layer structure, hence reducing the mechanical properties. Therefore, it is imperative to understand the stability of the multilayer thin film coating at higher temperature which allows the migration of the grain boundaries.

Pinching of the multilayer due to heat treatment have been observed in many different systems. In case of Silver (Ag)/ Silicon (Si) multilayer system with layer thickness between 3-5 nm, discontinuity in the layer has been observed after heat treatment above 600K [8]. They have also observed granular Ag at 723 K temperature. Layer pinching

*Corresponding authors

Email addresses: tchakrabarti@mines.edu (Tamoghna Chakrabarti), smanna@mines.edu (Sukriti Manna)

in multilayer coating has been studied with analytical model by Wan et.al[9]. Thermal stability of Copper (Cu)-Tungsten (W) multilayer system with 5nm thickness has been studied by Moszner et.al. They have observed two main microstructural changes i.e. formation of line-shaped protrusions at the temperature higher than 500°C and degradation of the nanolayered structure at higher than 700°C. The initial multilayer structures completely disintegrate into a nanocomposite structure, comprising globular W particles embedded in a Cu matrix[10].

Our experimental Fig. 1 shows the microstructural evolution in Zirconium (Zr)/Zirconium Nitride (ZrN) multilayer thin film before and after the thermal treatment. The darker phases in Fig. 1 are Zr and brighter one are ZrN. The Focused Ion Beam (FIB) cross section of the multilayer is shown in Fig. 1a. Fig. 1c shows the cross sectional high angle annular dark field (HAADF)-TEM micrographs of the same multilayer before the heat treatment. Fig. 1b represents the layer structure after the heat treatment 973K where it is evident that the layer structure gets disrupted after the heat treatment and the nitride grows through the metal layer not as a parallel front rather through some grains. Fig. 1d shows that, even higher temperature heat treatment at 1173K completely disintegrates the layer structure. Residue of metal can be seen as few metal packets retained inside the nitride matrix after heat treatment at 1173K.

The above mentioned instability problem of nanocrystalline multilayer is in mesoscale length scale owing to the nanometer sized grains and layers. The mechanisms involved are atomic diffusion and grain boundary migration. Therefore, phase-field modeling technique is ideally suited to model this phenomenon [11]. The phase-field model can also allow different grain boundary mobility in different phases, which can play an important part in the temporal evolution of the system. Additionally, this modeling technique correctly captures the effect of curvature which plays a significant role in producing the Plateau -Rayleigh instability leading to disintegration of the layer structure. Phase-field modelling of Plateau-Rayleigh instability in nano-wire and systems with continuous porous channel have been studied previously [12, 13].

The goal of this work is to understand the underlying mechanism (or mechanisms) behind of layer instability that can arise in nanocrystalline multilayer thin film. Additionally, the effect of layer thickness, bilayer spacing and grain boundary mobility on the stability of the multilayer thin film are also extensively explored through phase-field technique.

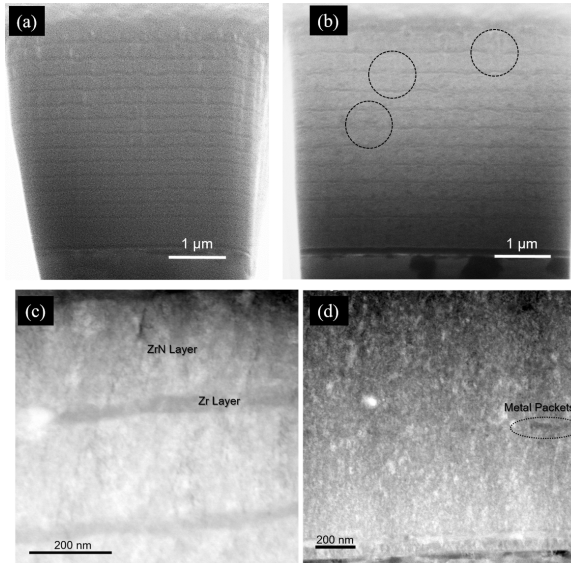


Figure 1: FIB cross sections showing layer structure at (a) 773K and (b) 973K for 250/50 nm multilayer coating. The interrupted layered structure is marked in (b). HAADF micrographs for as grown (c) and after 1173K (d), where the residual metal packets are marked in (d).

2. Methods

2.1. Experimental

Multilayer coating with bilayer spacing of 250/50 nm (ZrN/Zr) repeated for the total thickness of 5 μm were magnetron sputtered at TEER coating, UK. Heat treatments were done at 773-1173K for 1hr, for the thermal stability study. Heat treatments were done in a vacuum furnace at the heating rate of 10°C/min with samples vacuum sealed in a quartz tube to further reduce the oxygen content. Microstructure characterization of as-grown and heat treated samples were done by Focused Ion Beam (FIB, strata, FEI Inc., USA) and Transmission electron microscopy (TEM, Tecnai F-30, FEI Inc., USA). Cross-section imaging was used to image layers in secondary electron imaging mode in FIB. High angle annular dark field (HAADF) imaging was used to generate Z contrast images in TEM.

2.2. Computational

Our dual phase (α and β) polycrystalline multilayer system is described by three types of phase-field variables : c describes the chemical composition, η_i^α for $i = 1, 2, \dots, n_\alpha$ describes n_α unique grain orientations in the α phase and η_j^β for $j = 1, 2, \dots, n_j^\beta$ describes n_β unique grain orientations in the β phase. Chemical compositions of α and β phases are c_α and c_β respectively. The temporal evolution of microstructure is governed by the Cahn-Hilliard equation [14] and the Allen-Cahn equations [15]

$$\frac{\partial c}{\partial t} = \nabla \cdot M \nabla \mu \quad (1)$$

$$\frac{\partial \eta_i^\alpha}{\partial t} = -L_\alpha \frac{\delta(F/N_v)}{\delta \eta_i^\alpha} \quad (2)$$

$$\frac{\partial \eta_j^\beta}{\partial t} = -L_\beta \frac{\delta(F/N_v)}{\delta \eta_j^\beta} \quad (3)$$

where t is time, M is the atomic mobility (related to atomic diffusivity)

$$D = M \frac{\partial^2 F}{\partial c^2} \quad (4)$$

where F is the bulk free energy density defined below), L (L_α and L_β) is a relaxation coefficient for order parameter field η (grain boundary mobility) and μ is the chemical potential, defined as the variational derivative of the total free energy per lattice site, F , with respect to the local material density,

$$\mu = \frac{\delta(F/N_v)}{\delta c} \quad (5)$$

F is described by,

$$F = N_v \int_{\Omega} [f(c, \eta_i^\alpha, \eta_i^\beta) + \kappa_c (\nabla c)^2 + \sum_{i=1}^{n_\alpha} \kappa_\eta^\alpha (\nabla \eta_i^\alpha)^2 + \sum_{i=1}^{n_\beta} \kappa_\eta^\beta (\nabla \eta_i^\beta)^2] d\Omega \quad (6)$$

Our free energy function is constructed from free energy functional described by Fan et.al. and Poulsen et. al. [16, 17]. Our free energy functional f is described by,

$$\begin{aligned}
f(c, \eta_i^\alpha, \eta_i^\beta) = & \frac{A}{2}(c - c_m)^2 + \frac{B}{4}(c - c_m)^4 + \frac{D_\alpha}{4}(c - c_\alpha)^4 + \frac{D_\beta}{4}(c - c_\beta)^4 - \frac{G_\alpha}{2}(c - c_\beta)^2 \sum_{i=1}^{n_\alpha} (\eta_i^\alpha)^2 + \\
& \frac{d_\alpha}{4} \sum_{i=1}^{n_\alpha} (\eta_i^\alpha)^4 - \frac{G_\beta}{2}(c - c_\alpha)^2 \sum_{i=1}^{n_\beta} (\eta_i^\beta)^2 + \frac{d_\beta}{4} \sum_{i=1}^{n_\beta} (\eta_i^\beta)^4 + \frac{\epsilon}{2} \sum_{i=1}^{n_\alpha} (\eta_i^\alpha)^2 \sum_{j=1}^{n_\beta} (\eta_j^\beta)^2 + \\
& \epsilon_\alpha \sum_{i=1}^{n_\alpha} \sum_{j>i}^{n_\alpha} (\eta_i^\alpha)^2 (\eta_j^\alpha)^2 + \epsilon_\beta \sum_{i=1}^{n_\beta} \sum_{j>i}^{n_\beta} (\eta_i^\beta)^2 (\eta_j^\beta)^2
\end{aligned} \quad (7)$$

Here $c_m = (c_\alpha + c_\beta)/2$, $A, B, D_\alpha, D_\beta, G_\alpha, G_\beta, \epsilon, \epsilon_\alpha, \epsilon_\beta$ are constants. Dihedral angle between α phase and β phase grain boundaries in our model is 140° . We have used periodic boundary condition. Semi-implicit Fourier spectral method was used for solving kinetic equations [18]. Discrete Fourier transforms were performed using FFTW software package [19].

Table 1: Parameters Used in Simulations

Parameters	Non dimensional Values
C_α	0.05
C_β	0.95
A	2.00
B	9.80
D_α, D_β	1.52
G_α, G_β	1.23
d_α, d_β	1.00
$\epsilon, \epsilon_\alpha, \epsilon_\beta$	7.00
κ_c	0.75
κ_η^α	1.25
κ_η^β	1.00
$\Delta x, \Delta y$	2.00
Δt	0.20

3. Results and Discussions

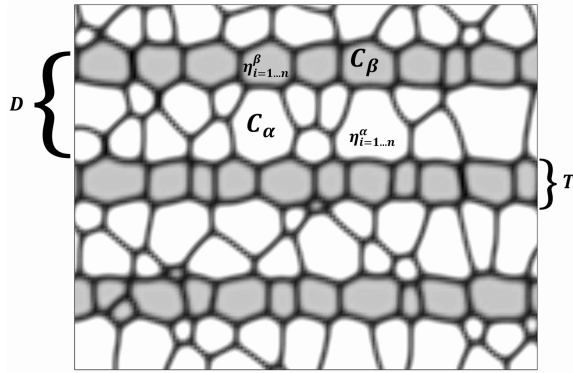


Figure 2: Two dimensional schematic of multi layer thin film, showing two different layer compositions and order parameters as well as β layer thickness (T), and bilayer thickness (D).

Fig. 2 shows the schematic of the multilayer thin film studied in this work. C_α and C_β are the compositions of two alternate layers. We have not applied any external perturbation at $\alpha - \beta$ interface in this study. In general, our β layer thickness is lower than that of the α layer.

3.1. Mechanism of Film Disintegration

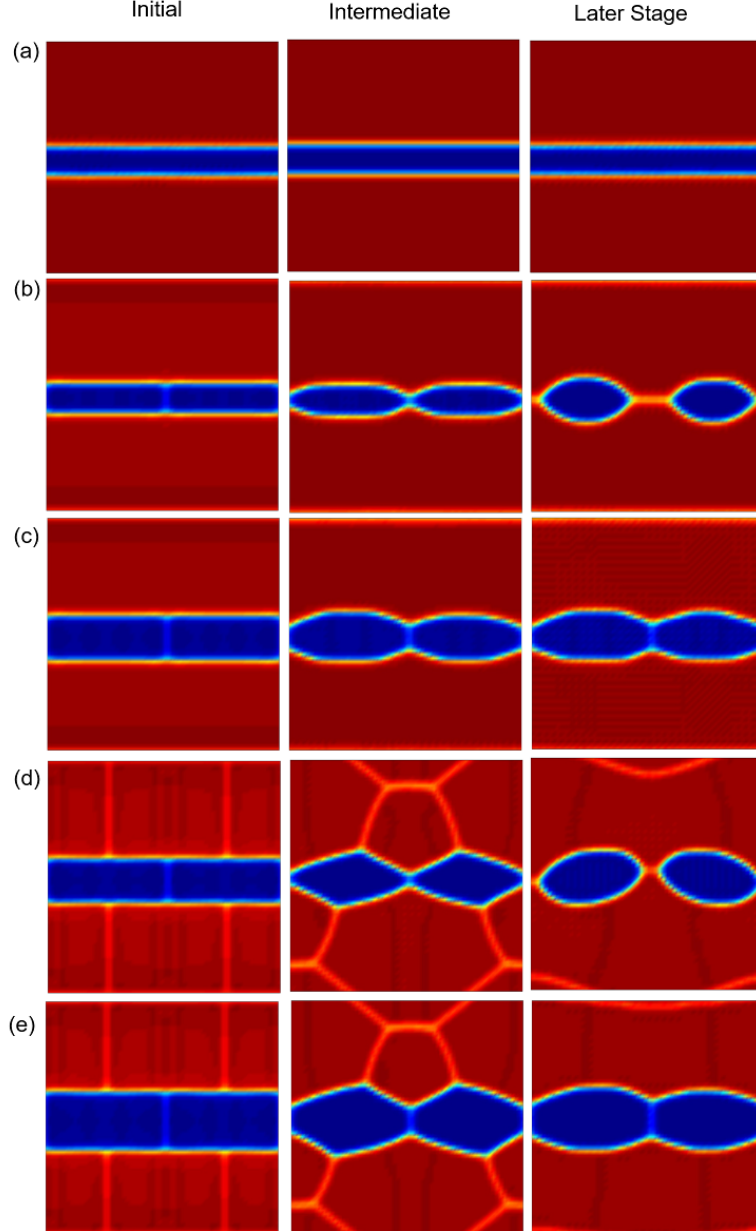


Figure 3: Early, intermediate and final stage of evolution in (a) single crystal multilayer thin film with $T = 8$, (b) polycrystalline layer embedded in single crystal layer of thickness $T = 16$ and (c) $T = 24$, (d) polycrystalline layer embedded in polycrystalline layer of thickness $T = 24$ and (e) $T = 32$. Here α and β layers are described by red and blue colors respectively

To understand the underlying mechanism behind the film disintegration, we have studied an idealized system with 128x128 system size with alternate layers of α and β phase. We have varied the β layer thickness (T) from 16 to 40.

3.1.1. Case I: Both the layers are Amorphous (or single crystal)

For any thickness of β layer no rupture in β layer is observed when both the layers are amorphous or single crystal (Fig. 3a). This suggests that when the layers are devoid of grain boundaries they are stable. As we have mentioned earlier that we have not imposed any perturbation in this study.

3.1.2. Case II: Presence of Grain Boundaries in one (α or β) layer

In this situation, we have observed rupture in β layer at the later stage when $T = 16$ (Fig. 3b). Presence of grain boundary in β layer causes grain grooving which leads to perturbation in the α - β interface. This perturbation grows over time and finally ruptures the β layer. Thus the α phase grows between two β grains at the later stage. Therefore, the presence of grain boundary in β layer (or α) makes it less stable than Case I. But, Fig. 3c, shows at higher thickness of ($T = 24$), the β layer remains stable.

3.1.3. Case III: Presence of Grain Boundaries in both α and β layer

Fig. 3d, shows the result of polycrystalline β layer of ($T = 24$) embedded in polycrystalline α . Presence of grain boundaries in both α and β phases makes it more unstable (Fig. 3d) than the previous two cases as rupture of β layer is observed even at $T = 24$. The grain boundary at the middle of the β layer causes grain grooving just as before, but the grain boundary of α phase also experiences grain grooving in reverse directions. This can be explained by Plateau-Rayleigh instability (PR)[20].

$$KT_E < 1 \quad (8)$$

$$K = \frac{2\pi}{\lambda} \quad (9)$$

$$\lambda = G \quad (10)$$

$$T_E < \frac{\lambda}{2\pi} \quad (11)$$

$$T_E < \frac{G}{2\pi} \quad (12)$$

According to PR instability, the layer becomes unstable when $KT_E < 1$, where K is the wave number and T_E is the effective thickness of the β layer and G is grain size. Due to grain grooving, effective thickness T_E is always lower than the starting thickness T . For our simulation parameters, PR instability will make the layer unstable when $T_E < 10$ as shown by equation 12. Fig. 4 shows the corresponding schematics which elaborates the formation of sinusoidal perturbation due to the grain grooving. Owing to grooving on the both side of the β layer, T_E is 8 (< 10) in case of $T = 16, 24$ and layer ruptures. We observe that the layer remains stable when $T_E > 10$ in case of $T = 32$ (i.e. $T_E = 16$). Therefore, our simulations corroborates with the Plateau-Rayleigh instability criterion.

Polycrystallinity in the two phases also affects the kinetics of the disintegration of β layer. For the polycrystalline film embedded in single crystal of thickness ($T = 16$) (Fig. 3b), takes much longer time to rupture (Time = 1800), compared to polycrystalline film embedded in polycrystalline layer (Time = 600) of the same thickness. Polycrystalline α and β film of ($T = 16$) takes around three times lesser time (Time = 600) to rupture than film of thickness $T = 24$ (Time = 1800).

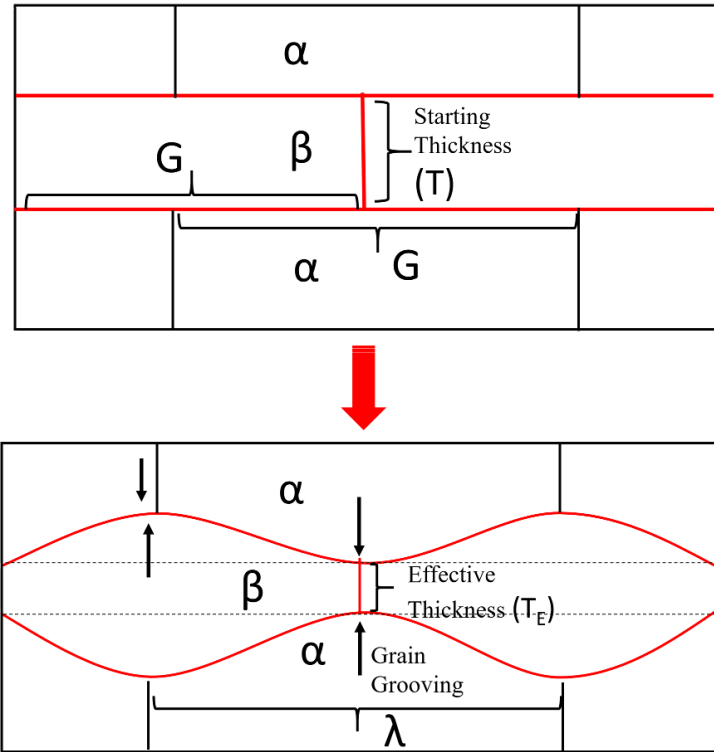


Figure 4: Schematics of early and final stages of multilayer thin film. Arrows showing the direction of grain grooving.

3.2. Factors Affecting the Stability of Thin Film :2D System

From here onwards we have discussed the evolution of 2D multilayer thin film with system size of 1024x1024.

3.2.1. Microstructural Evolution with Time

We will start the result section with the microstructural evolution of the multilayer thin films. Fig. 5 a-d show the snapshots of the film disintegration for $T = 16$. The β layer starts to pinch off at Time = 200. The α phase grows through the β layer. This microstructure looks similar to the microstructure we have observed in Zr/ZrN multilayer after the heat treatment at 973K shown in Fig. 1b. With the evolution of time, the β layer gets visibly more disintegrated as shown in Fig. 5c. Finally, the layers becomes isolated islands of β phase in Fig. 5d. We observe similar isolated pockets of Zr metal after heat treatment at 1173K (Fig. 1d). Higher β layer thickness slows down the kinetics but the microstructural evolution trajectory remains same as seen for $T = 16$.

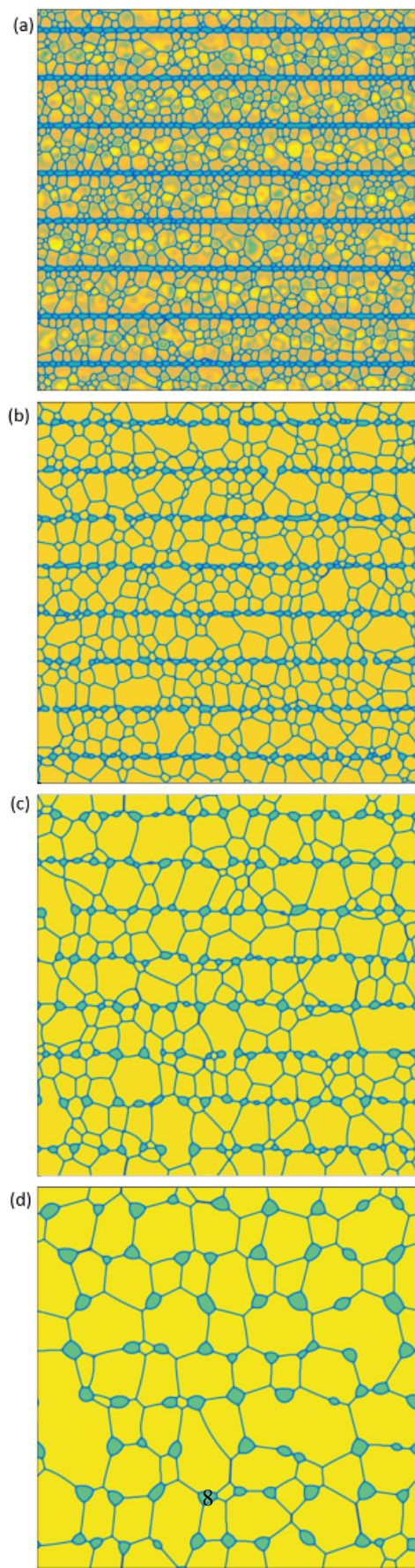


Figure 5: Microstructural evolution of multilayer thin film at (a) Time = 100, (b) Time = 500, (c) Time = 1700 and (d) Time = 10000.

3.2.2. Effect of Film Thickness

Fig. 6a-g show the initial configuration whereas Fig. 6a'-g' show the final configuration after Time = 10000. In the Fig. 6 a-d, from left to right β layer thickness increases from 16 to 40. Final configurations a'-c' show that as we move from $T = 16$ to $T = 32$ the extent of β layer disintegrity decreases. At $T = 16$, the β film layer is least stable whereas when $T = 40$, β layer is totally stable. For $T = 16$, The β phase exists as droplet shape in grain boundaries or grain boundary triple points of α phase. Dependence of layer stability of layer thickness has been shown experimentally by Misra et. al. in nanocrystalline Copper (Cu)-Niobium (Nb) multilayer system[21].

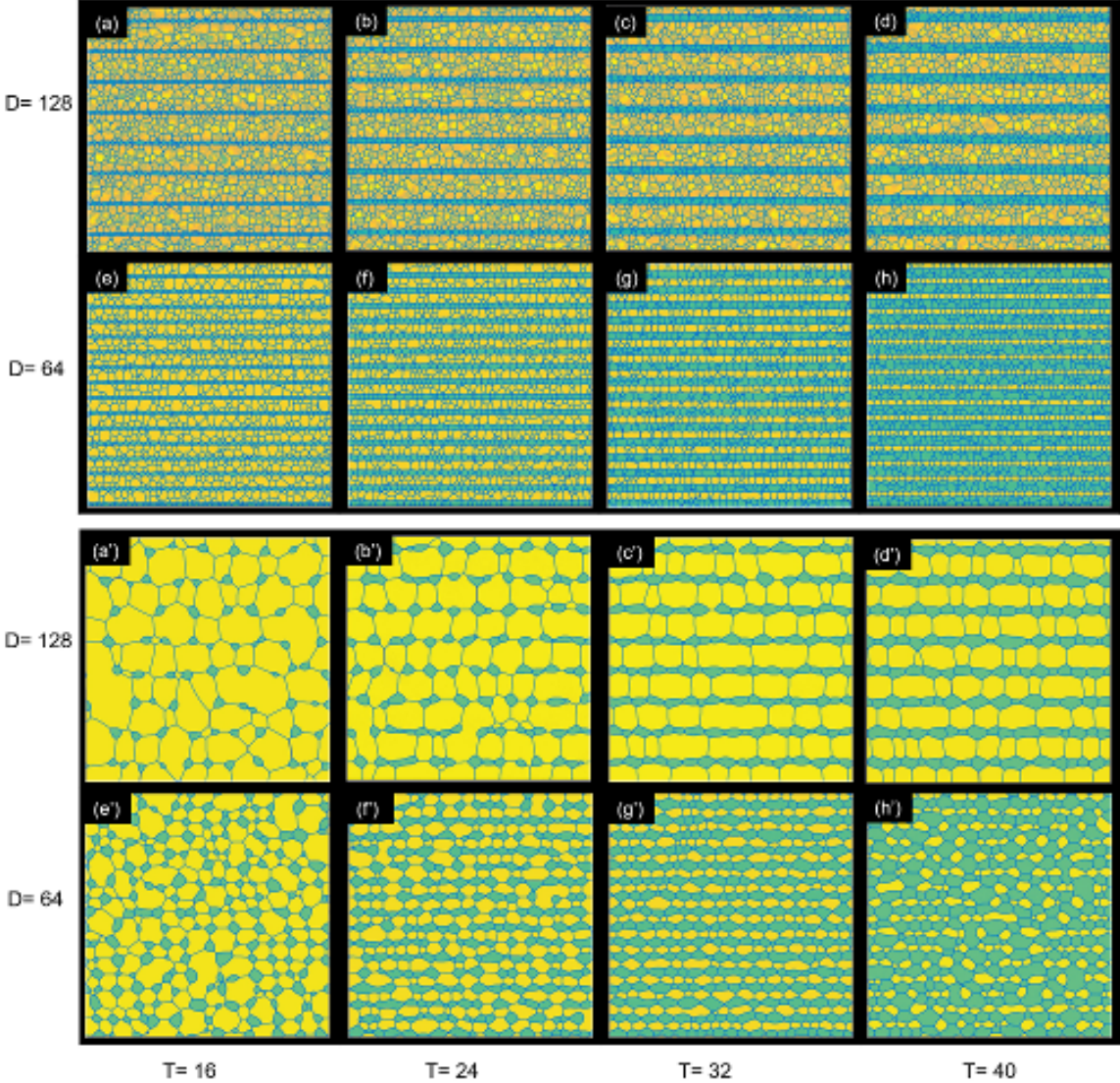


Figure 6: Early stage (Time = 100) and final stage (Time = 10000) microstructures of multilayer thin film with different layer thickness (T), and bi-layer thickness (D).

As with the small system with idealized configuration described in Fig. 3, here also the kinetics of film disintegration is controlled by layer thickness. Thicker film layer takes significantly longer time to break. Table 2 shows the film thickness and time to break comparison.

We have also studied the coarsening kinetics of the grains in individual α and β phase. Fig. 7 a and 7 b show the grain coarsening with time in α and β layer respectively. Grain size has been computed using Hoshen-Kopelman

Table 2: β layer thickness vs Time to Disintegrate

Film Thickness	Time (D = 128)	Time (D = 64)
T = 16	200	300
T = 24	1000	2200
T = 32	3500	8400
T = 40	Does not break	α Layer breaks

algorithm [22] at each time step. As, α layer thickness decreases with increasing β layer thickness (T), correspondingly we observe monotonous decrease in final α grain area. α and β grains only grow as large as the corresponding layer thickness therefore grain size is dictated by their layer thickness. In all the four cases (T = 16, 24, 32 and 40), the grain area vs time plot of α phase shows two distinct stages. Initially, grains coarsen at much higher rate and then slows down significantly. This is because initially grains coarsen freely inside each individual layer without much hindrance as the number of the grain boundaries pinned by the grain grooving are much smaller than the total number of the grain boundaries. At this stage, grain coarsening is independent of the layer thickness and coarsening rate remains the same in all the four cases. After some time, morphology of the grains change to columnar. Grain boundary of those columnar grains are pinned by the grain grooves on both the sides. Mechanism of grain boundary pinning by the grooves are discussed by Mullins et.al.[23] This pinning effect slows down the grain coarsening rate significantly. Therefore, we observe a crossover to much slower coarsening regime in the Fig. 7 a. As, the α layer is thinner with increasing β layer thickness (T), the crossover point to columnar grains arrive sooner. Consequently, the cross over point between the faster and slower coarsening regime is shifted to the left.

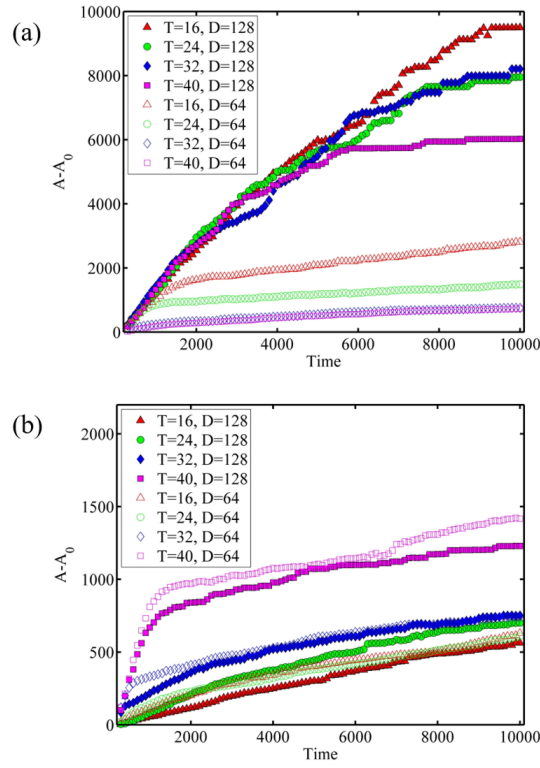


Figure 7: Average grain area in (a) α layer and (a) β layer vs time plot for different β layer thickness (T) and bi-layer thickness (D).

Fig. 7 b shows the grain coarsening behavior with time in β layer. As in α layer, β layer grain area shows monotonous increase with increasing layer thickness. Here, in case of T = 16, 24 and 32, grain area vs time plot do

not show two distinct regimes. Because of its lower thickness grain coarsening produces columnar grains in β layer earlier than α layer (before time 200). Therefore, fast coarsening regime can not be seen. But, for $T = 40$, as the thickness is higher, a fast coarsening regime can be observed which is analogous to the coarsening in the α layer.

3.2.3. Formation of Columnar Grains

Due to the slower movement of some grain boundaries (at $\alpha - \beta$ interface) by grain grooving and faster grain boundary (at individual α or β grain boundaries) movement elsewhere, columnar grains will always arise in thin film eventually, provided the non-pinned boundaries can move. This observation can explain the reason behind the columnar grains formation in the nano-crystalline thin film produced experimentally [24]. Sequence of the grain boundary migration and columnar grain formation is shown in Fig. 8. Columnar grain arises in both α and β layer. It also can be observed that the columnar grain arises much earlier in β layer owing to lower film thickness.

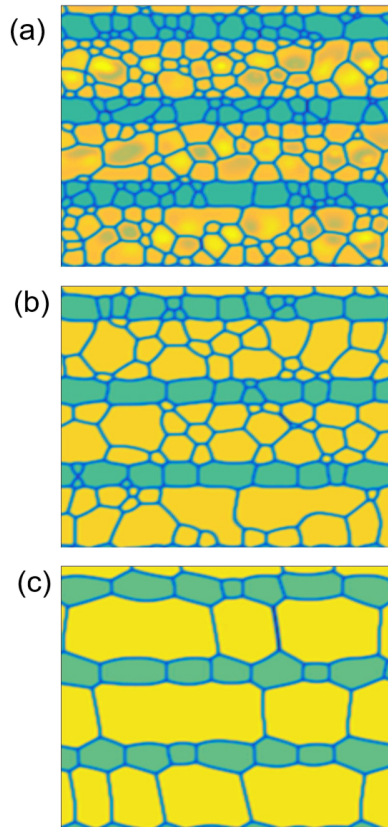


Figure 8: Micrograph showing evolution of grain structures with time, (a) Time = 100, (b) Time = 400 and (c) Time = 4000 . Here yellow and green colored grains represents α and β layers respectively.

3.2.4. Effect of Bi-Layer Thickness (D)

Here we have discussed the effect D on the stability of β layer. In the Fig. 6, from left to right β layer thickness increases from 16 to 40 and top row shows result from bi-layer thickness of 128 and bottom layer shows the result from bi-layer thickness of 64. The initial configuration is shown in Fig. 6 a-g whereas Fig. 6 a'-g' show the final configuration after Time = 10000.

In the Fig. 6, top and bottom micrographs show the result of the same β layer thickness but with different bi-layer thickness. Higher D values means higher α layer thickness and less number of layers. For higher D values, the time to layer disintegration is lower for the same β layer thickness T which is shown in Table 2. This can be explained through PR instability. For higher D , α layer thickness is higher and resultantly, grain sizes are much larger as shown in Fig. 7 a. This corresponds to higher wavelength (λ) of perturbation as shown by Eq. 10. For the same β layer

thickness, higher λ leads to the faster disintegration of the β layer [12]. Therefore, higher bi-layer thickness, virtue of larger α phase grain size and correspondingly higher λ leads to faster disintegration of the multilayer. In case of the $T = 40$ and $D = 64$, α layer becomes discontinuous as the α layer thickness (24) is lower than the β layer.

Fig. 7 a, b show the grain coarsening with time in α and β layer respectively. As, α layer thickness increases with higher bi-layer thickness (D), final grain area increases. In all the four cases (i.e. $T = 16, 24, 32$, and 40), the grain area vs time plot shows similar trends. Fig. 7 b shows the grain coarsening with time in β layer. For β layer, thicknesses (T) is the same for $D = 64$ and 128 . Here, grain area vs time shows similar trajectory in both the cases.

3.2.5. Effect of Grain Boundary Mobility (L)

In this section we have discussed the effect of grain boundary mobility (L) on the stability of the multilayer thin film. Table 3 shows the L_α and L_β and the corresponding time to break. For the multilayer film with β layer thickness $T = 16$ and 24 time to break increases with lower L_α and L_β . Instability in this film originates from the grain grooves. Formation of grain grooves depends on the movement of grain boundaries which is controlled by the parameter L. Therefore, it is natural that with lower values of L (L_α and L_β) hinders the kinetics of film disintegration.

Lowering of α phase grain boundary mobility L_α keeping L_β constant affects the time to breakage of β layer more than the vice-versa for both $T = 16$ and 24 . Higher α phase grain boundary mobility L_α , means larger grain size of α which increases the λ (as shown by Eq. 10) and leads to the faster disintegration of the β layer. This effect is similar to the effect of larger D value discussed previously.

Table 3: Grain boundary mobility (L) vs Film Disintegration Time

Film Thickness	Time (T = 16)	Time (T = 24)
$L_\alpha = 1.00, L_\beta = 1.00$	200	1000
$L_\alpha = 0.10, L_\beta = 0.10$	300	1600
$L_\alpha = 0.01, L_\beta = 0.01$	800	3800
$L_\alpha = 1.00, L_\beta = 0.01$	500	2500
$L_\alpha = 0.01, L_\beta = 1.00$	700	3800

Fig. 9 and 10 show the grain coarsening with time in α and β layer and $T = 16$ and $T = 24$ respectively. α and β layer grain size increases with higher values of respective L. In all the cases (i.e. $T = 16$ and 24), the grain area vs time plot shows similar trend. α layer grain size is more dependent on L_α compared to the β phase on L_β . This is because, the grain boundaries in the β phase are constrained by grain grooving from very early stage owing to lower thickness and therefore controlled by movement of pinned boundary which depends on bulk diffusion in addition to L values and moves at significantly slower rate.

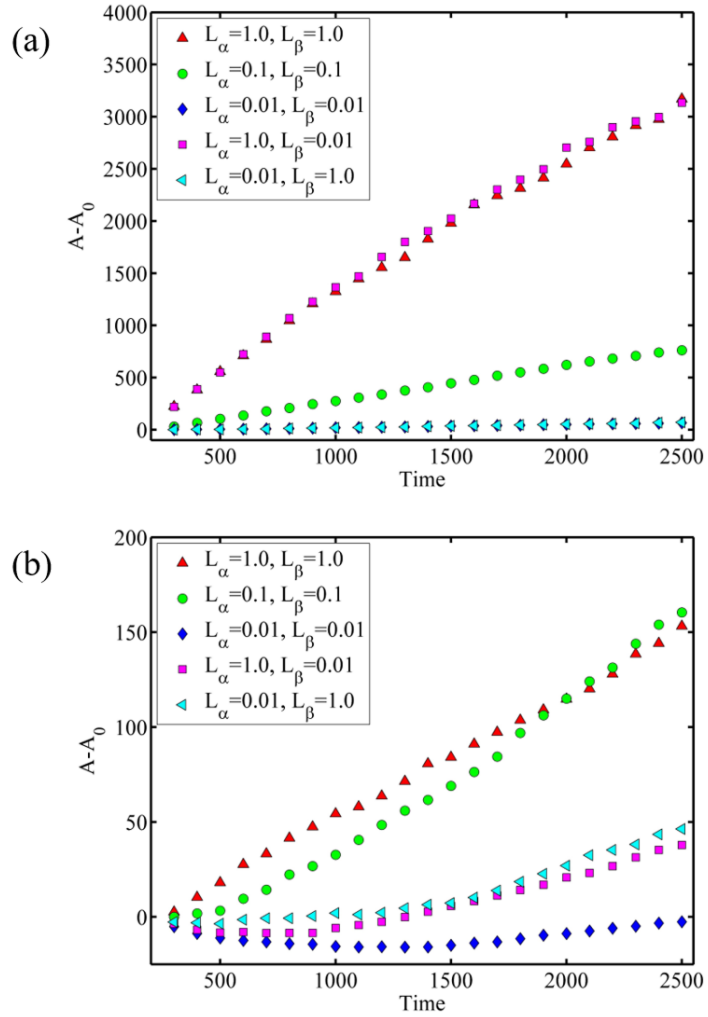


Figure 9: Average grain area in (a) α and (b) β layer vs time plot for $T = 16$ and different L .

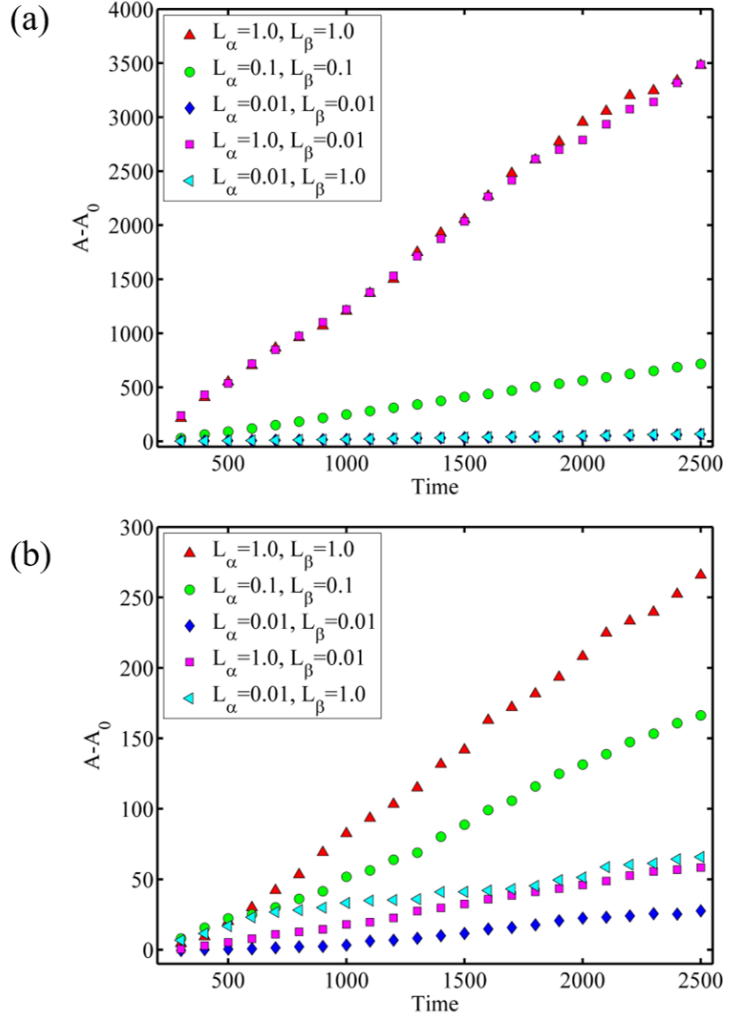


Figure 10: Average grain area in (a) α and (b) β layer vs time plot for $T = 24$ and different L .

Multilayer thin films in use today, mostly contain alternate layers of metal and ceramic. Our simulation results show that the metal layer due to its higher grain boundary mobility (L), will be more susceptible to disintegration than the ceramic layer. Our model also indicates that the grain boundary mobility (L) of the ceramic phase has strong influence on the rupture of the metal layer. Faster the L is in ceramic layer, faster the metal layer will disintegrate.

To avoid the disintegration of the metal layer, it should be as thick as possible. Also, bi-layer thickness should be as low as possible without causing disruption in the ceramic layer. This is because, lower bilayer thickness with higher thickness of metal means lower thickness of ceramic layer. Ceramic layer by virtue of its much lower L , can resist the disintegration even at a thickness much lower than the metal layer.

Ceramic layer also should have as low grain boundary mobility as possible as the grain boundary mobility of ceramic layer affects the metal layer disintegration. As grain boundary mobility is a strong function of melting point, higher melting point ceramic will be better for multilayer stability. Similarly, constituent metal of the metal layer also should have higher melting point (i.e. lower grain boundary mobility) to achieve higher thermal stability.

3.2.6. Presence of Amorphous Layer

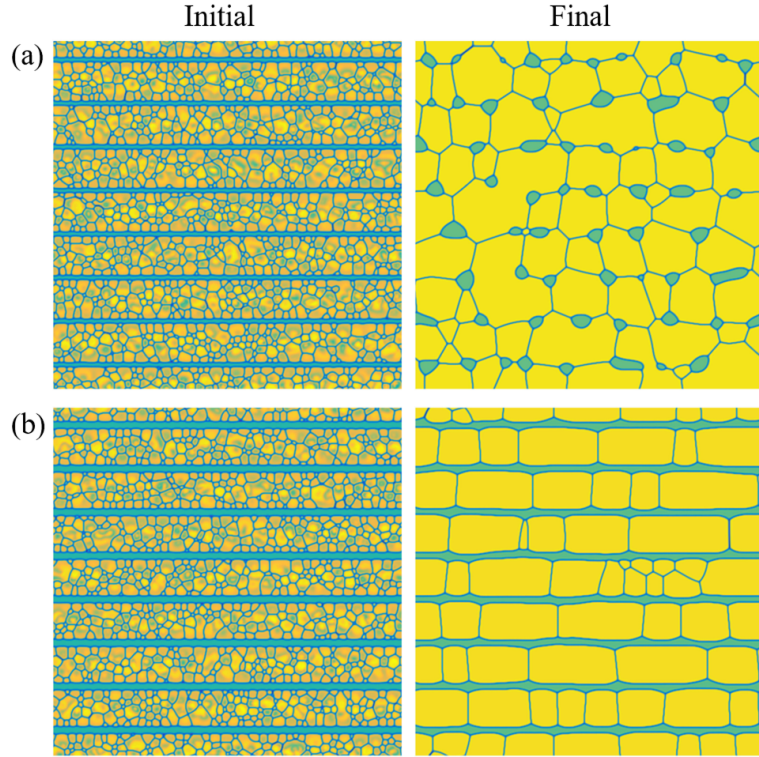


Figure 11: Initial (Time = 0) and later stage microstructures of multilayer thin film with different layer thickness is shown in (a) $T = 16$, and (b) $T = 24$

In multilayer coating, some time amorphous layer is formed due to kinetic reason [25]. Therefore, an important aspect of this study is their thermal stability. In our model, amorphous layers are those which do not have any grain boundaries. The same can be attributed to single crystal layer as well. Basically, in our model there are no differences between amorphous and single crystal layer. The result of micro-structural evolution in those systems has been shown in Fig. 11. Here, we have discussed microstructural evolution of the alternate amorphous and polycrystalline layer. If both the layers are amorphous, our small system size has already shown that layers are stable for any thickness as without the grain boundaries and corresponding grooving there are no differential curvature which can lead to disintegration of the layer. We have kept D to 128. The Fig. 11 shows that rupture of the multilayer occurs for $T = 16$ but not for $T = 24$ till the simulation time of 10000. We have observed the same in our small system size simulations as well. Time to rupture in this case i.e. amorphous β layer is 600 which is three time longer than in case of the polycrystalline β layer. Clearly, grain boundaries in polycrystalline layer makes rupture easier and faster. Slower disintegration of single crystal gold nanowire due to the PR instability has been observed experimentally as well[26]. Additional curvature from polycrystalline material due to grain grooving is likely responsible for such phenomenon as shown by our modelling results.

3.3. Stability of Thin Film : 3D System

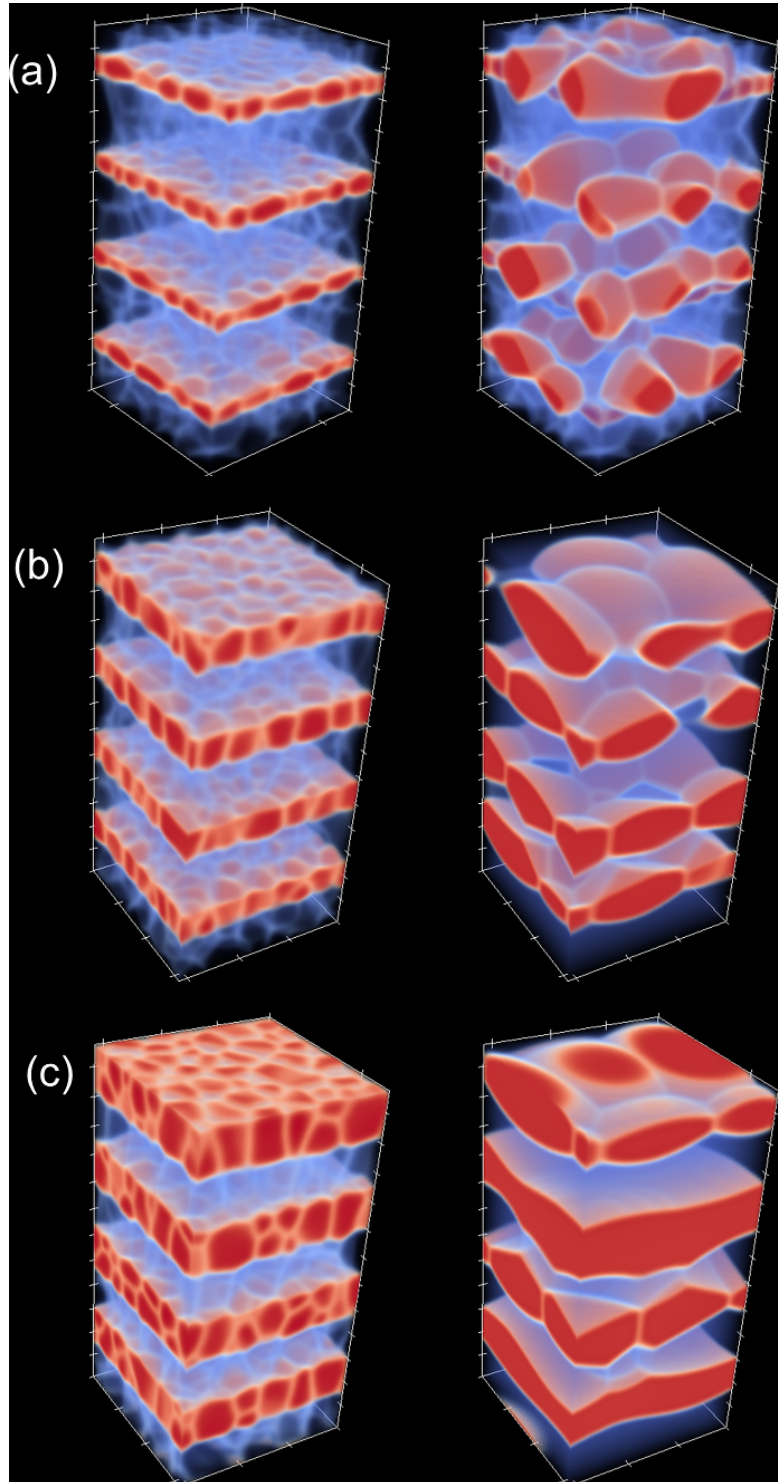


Figure 12: Initial (Time = 0) and later stage microstructures of multilayer thin film with different layer thickness is shown in (a) $T = 16$, (b) $T = 24$ and (c) $T = 32$. β layers are shown in red. In the α layers only grain boundaries are shown for clarity.

Result of the phase field simulation of multilayer thin film in 3D is shown in Fig. 12. For 3D simulation system, size of 256x128x128 is taken. Bilayer thickness (D) is fixed to 64 and the thickness of β layer is varied from 16-32. Fig. 12 shows rupture in thin film in case of $T = 16$ and 24. For $T = 32$, any rupture is not seen up to the time of 6000. In case of $T = 16$, layer rupture starts at time 100. Time taken to rupture is longer in case of $T = 24$ i.e. 1300. In comparison to the 2D system time taken to rupture in multilayer thin film is lower in 3D system. Additional curvature in 3D system is likely responsible for such a reduction. Layer rupture is not observed for $T = 32$, till the simulation time of 5000. Due to the computational resource constraint, longer simulation was not tried. Incidentally for the same configuration, 2D simulation took 8400 time to show first sign of the rupture. Significant grain coarsening and columnar grain formation is observed in all the above mentioned cases which is analogous to the result we have seen in the 2D system.

4. Conclusion

In the course of this work we have investigated various factors that affects the stability of the nano-crystalline multilayer thin film. The instability in such a film has been discussed on the basis of two interconnected phenomena : grain grooving and PR instability. Grain grooving, which arises from the polycrystalline nature of the film that introduces a variation in curvature at different region of the film. This differentiallity in curvature (perturbation) leads to the rupture of the film due to PR instability.

Our phase-field simulation helps to predict the role of different parameters on the film disintegration. Thickness of the film is the most important parameter. Beyond a particular thickness we do not observe an evidence of film disintegration. This thickness in case of polycrystalline multilayer thin film is higher than the thickness predicted by PR instability criteria, as the grain boundary grooving reduces the effective thickness (T_E) of the film.

Grain boundary migration controls the grain grooving which in turn is responsible for the breaking in the multi-layer thin film. So, in material with lower grain boundary mobility will take longer time to break up. As, increasing the temperature increases the grain boundary mobility, multi-layer thin film will be more susceptible to rupture at elevated temperatures as shown by our experimental results as well in Fig. 1.

Increasing the thickness of the multilayer thin film is always not a viable option to prevent film disintegration. Since, increasing layer thickness also increase the grain size which may reduce the strength of the film by Hall-Petch effect [27, 28]. Reducing the bi-layer thickness also reduces kinetics of film disintegration. Making one of the layer amorphous or single crystal will be another way to prevent instability in the thin film.

References

- [1] L. Hultman, Thermal stability of nitride thin films, *Vacuum* 57 (1) (2000) 1–30.
- [2] J. Xu, K. Hattori, Y. Seino, I. Kojima, Microstructure and properties of crn/si 3 n 4 nano-structured multilayer films, *Thin Solid Films* 414 (2) (2002) 239–245.
- [3] E. Bozyazı, M. Ürgen, A. F. Çakır, Comparison of reciprocating wear behaviour of electrolytic hard chrome and arc-pvd crn coatings, *Wear* 256 (7) (2004) 832–839.
- [4] K. Shih, D. Dove, Ti/ti-n hf/hf-n and w/w-n multilayer films with high mechanical hardness, *Applied physics letters* 61 (6) (1992) 654–656.
- [5] N. Verma, V. Jayaram, Detailed investigation of contact deformation in zrn/zr multilayer—Understanding the role of volume fraction, bilayer spacing, and morphology of interfaces, *Journal of Materials Research* 28 (22) (2013) 3146–3156.
- [6] A. Madan, X. Chu, S. Barnett, Growth and characterization of epitaxial mo/nbn superlattices, *Applied physics letters* 68 (16) (1996) 2198–2200.
- [7] A. Madan, Y.-y. Wang, S. Barnett, C. Engström, H. Ljungcrantz, L. Hultman, M. Grimsditch, Enhanced mechanical hardness in epitaxial nonisostructural mo/nbn and w/nbn superlattices, *Journal of applied physics* 84 (2).
- [8] K. Kapta, A. Csik, L. Daroczi, Z. Papp, D. Beke, G. Langer, A. Greer, Z. Barber, M. Kis-Varga, Degradation of ag/si multilayers during heat treatments, *Vacuum* 72 (1) (2003) 85–89.
- [9] H. Wan, Y. Shen, X. He, J. Wang, Modeling of microstructure evolution in metallic multilayers with immiscible constituents, *JOM* 65 (3) (2013) 443–449.
- [10] F. Moszner, C. Cancellieri, M. Chiodi, S. Yoon, D. Ariosa, J. Janczak-Rusch, L. Jeurgens, Thermal stability of cu/w nano-multilayers, *Acta Materialia* 107 (2016) 345–353.
- [11] R. Mukherjee, T. Chakrabarti, E. A. Anumol, T. A. Abinandanan, N. Ravishankar, Thermal stability of spherical nanoporous aggregates and formation of hollow structures by sintering—a phase-field study, *ACS nano* 5 (4) (2011) 2700–2706.
- [12] C. Joshi, T. Abinandanan, A. Choudhury, Phase field modelling of rayleigh instabilities in the solid-state, *Acta Materialia* 109 (2016) 286–291.
- [13] F. Wang, B. Nestler, Detachment of nanowires driven by capillarity, *Scripta Materialia* 113 (2016) 167–170.
- [14] J. W. Cahn, On spinodal decomposition, *Acta metallurgica* 9 (9) (1961) 795–801.

- [15] S. M. Allen, J. W. Cahn, A microscopic theory for antiphase boundary motion and its application to antiphase domain coarsening, *Acta Metallurgica* 27 (6) (1979) 1085–1095.
- [16] D. Fan, L.-Q. Chen, S. Chen, P. W. Voorhees, Phase field formulations for modeling the ostwald ripening in two-phase systems, *Computational materials science* 9 (3) (1998) 329–336.
- [17] S. O. Poulsen, P. Voorhees, E. M. Lauridsen, Three-dimensional simulations of microstructural evolution in polycrystalline dual-phase materials with constant volume fractions, *Acta Materialia* 61 (4) (2013) 1220–1228.
- [18] J. Zhu, L.-Q. Chen, J. Shen, V. Tikare, Coarsening kinetics from a variable-mobility cahn-hilliard equation: Application of a semi-implicit fourier spectral method, *Physical Review E* 60 (4) (1999) 3564.
- [19] M. Frigo, S. G. Johnson, Fftw: An adaptive software architecture for the fft, in: *Acoustics, Speech and Signal Processing, 1998. Proceedings of the 1998 IEEE International Conference on*, Vol. 3, IEEE, 1998, pp. 1381–1384.
- [20] J. W. Strutt, L. Rayleigh, On the instability of jets, *Proc. London Math. Soc* 10 (4).
- [21] A. Misra, R. Hoagland, Effects of elevated temperature annealing on the structure and hardness of copper/niobium nanolayered films, *Journal of materials research* 20 (08) (2005) 2046–2054.
- [22] J. Hoshen, R. Kopelman, Percolation and cluster distribution. i. cluster multiple labeling technique and critical concentration algorithm, *Physical Review B* 14 (8) (1976) 3438.
- [23] W. Mullins, The effect of thermal grooving on grain boundary motion, *Acta metallurgica* 6 (6) (1958) 414–427.
- [24] J. A. Thornton, Influence of apparatus geometry and deposition conditions on the structure and topography of thick sputtered coatings, *Journal of Vacuum Science & Technology* 11 (4) (1974) 666–670.
- [25] D. Singh, X. Deng, N. Chawla, J. Bai, C. Hubbard, G. Tang, Y.-L. Shen, Residual stress characterization of al/sic nanoscale multilayers using x-ray synchrotron radiation, *Thin Solid Films* 519 (2) (2010) 759–765.
- [26] S. Karim, M. Toimil-Molares, W. Ensinger, A. Balogh, T. Cornelius, E. Khan, R. Neumann, Influence of crystallinity on the rayleigh instability of gold nanowires this paper is dedicated to professor dr h fueß on the occasion of his 65th birthday., *Journal of Physics D: Applied Physics* 40 (12) (2007) 3767.
- [27] E. O. Hall, The deformation and ageing of mild steel: Iii discussion of results, *Proceedings of the Physical Society. Section B* 64 (9) (1951) 747.
URL <http://stacks.iop.org/0370-1301/64/i=9/a=303>
- [28] N. Petch, The cleavage strength of polycrystals, *J. Iron Steel Inst.* 174 (1953) 25–28.